physica pss status solidi

www.interscience.wiley.com

reprints

www.pss-rapid.com

www.pss-c.com

www.pss-b.com

www.pss-a.com

WILEY-VCH

REPRINT

Phys. Status Solidi B **247**, Nos. 11–12, 2968–2973 (2010) / **DOI** 10.1002/pssb.201000151

physica status solidi b
www.pss-b.com
basic solid state physics

1D goes 2D: A Berezinskii–Kosterlitz–Thouless transition in superconducting arrays of 4-Angstrom carbon nanotubes

Zhe Wang, Wu Shi, Hang Xie, Ting Zhang, Ning Wang, Zikang Tang, Xixiang Zhang†, Rolf Lortz, and Ping Sheng*

Department of Physics and William Mong Institute of Nano Science and Technology, Hong Kong University of Science and Technology, Clear Water Bay, Kowloon, Hong Kong, China

Received 28 April 2010, revised 26 August 2010, accepted 27 August 2010
Published online 4 October 2010

Keywords 1D to 3D crossover, Berezinskii–Kosterlitz–Thouless transition, nanotubes, superconductivity

* Corresponding author: e-mail sheng@ust.hk, Phone: +852 2358 7474, Fax: +852 2358 1652
† Present address: Research and Development, King Abdullah University of Science and Technology, Thuwal, Saudi Arabia

We report superconducting resistive transition characteristics for array(s) of coupled 4-Angstrom single wall carbon nanotubes embedded in aluminophosphate-five zeolite. The transition was observed to initiate at 15 K with a slow resistance decrease switching to a sharp, order of magnitude drop between 7.5 and 6.0 K with strong (anisotropic) magnetic field dependence. Both the sharp resistance drop and its attendant nonlinear IV characteristics are consistent with the manifestations of a Berezinskii–Kosterlitz–Thouless transition that establishes quasi long range order in the plane transverse to the *c*-axis of the nanotubes, leading to an inhomogeneous system comprising 3D superconducting regions connected by weak links. Global coherence is established at below 5 K with the appearance of a well-defined supercurrent gap/low resistance region at 2 K.

Superconductivity in carbon nanotubes has been controversial because carbon is not known to be a superconducting element, and if there is indeed superconducting tendency in carbon nanotubes [1] (the large curvature of small carbon nanotubes can potentially open electron–phonon couplings that are absent in the graphene sheet, thereby enhancing the prospect for superconductivity), its manifestation could be quenched by long wavelength thermal fluctuations as well as by the Peierls distortion that favors an insulating ground state. In this context the earlier report on the Meissner effect in 4-Angstrom carbon nanotube–zeolite composites [2] and the more recent observation of their superconducting specific heat signals [3] have only deepened the mystery on the specific manner in which the nanotube superconductivity comes into being, and on whether there can be a sharp superconducting resistive transition that is usually taken to be the hallmark of a superconductor. Here we show that by devising strategy to make surface electrical contacts to the samples that are separated by only 100 nm, reliable and repeatable observations of the superconducting resistive transition can be obtained. The physical picture which emerges is that of a coupled Josephson array consisting of aligned nanotubes crossing over from an individually fluctuating 1D system to a coherent 3D superconductor, mediated by a Berezinkii–Kosterlitz–Thouless (BKT) transition [4, 5] which establishes quasi long range order in the transverse plane perpendicular to the *c*-axis of the nanotubes. The attainment of overall coherence across the measuring electrodes (denoted as global coherence in this work) is seen at 5 K and below, evidenced by the appearance of a well-defined (differential resistance) supercurrent gap/low resistance region at 2 K.

Figure 1 shows both a cartoon picture (Fig. 1a) of the aluminophosphate-five (AFI) zeolite crystal with the four-probe contact geometry, as well as a scanning electron microscope (SEM) image of an actual sample (Fig. 1b). Here the sample was prepared by first cutting two troughs in an AFI crystal ($50 \times 50 \times 500\,\mu m^3$) with focused ion beam (FIB, Seiko SMI2050), separated by a 5 μm slice that is perpendicular to the *c*-axis (Fig. 1a).

The straight pores of the AFI zeolite have a center-to-center separation of 1.37 nm, each with an inner diameter of 0.7 nm [6]. They form a 2D close-packed triangular lattice in

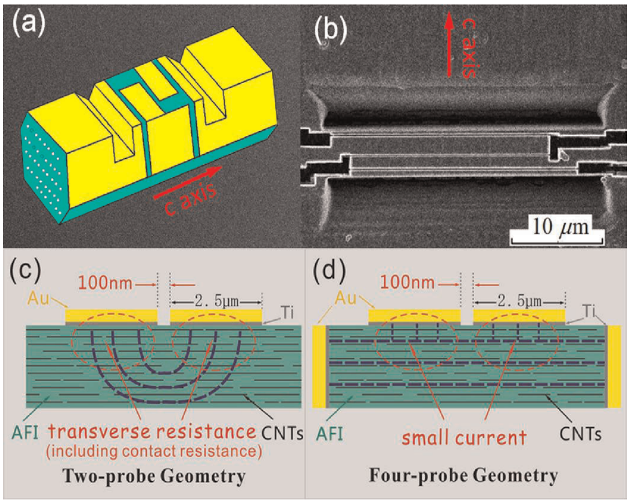

Figure 1 (online color at: www.pss-b.com) (a) Cartoon picture of the sample. Yellow denotes gold and green denotes AFI crystal surface exposed by FIB etching. Nanotubes are delineated schematically by open circles. (b) SEM image of the sample. The *c*-axis is along the N–S direction. The thin, light, horizontal line in the middle is the 100 nm separation between the two surface voltage electrodes that are on its two sides. The dark regions are the grooves cut by the FIB and sputtered with Au/Ti to serve as the end-contact current electrodes. (c) and (d) show schematic drawings of the two-probe and four-probe geometries, respectively. Blue dash lines represent the current paths. The two end-contact current pads in (d) are 4 μm in depth and 30 μm in width.

the plane transverse to the *c*-axis. The 4-Angstrom diameter nanotubes are embedded in the AFI zeolite pores (direct TEM visualization is reported in Ref. [7]). There can be three types of 4-Angstrom carbon nanotubes that are consistent with optical and Raman data [8–11]: (5,0), (4,2), and (3,3). We attribute the superconducting behavior to the (5,0) nanotubes.

The AFI zeolite crystal with embedded nanotubes [12] was sputtered with 50 nm of Ti and 150 nm of Au. The electrical contact geometry was subsequently delineated by using the FIB to remove the Au/Ti film in a pre-designed pattern (Fig. 1b). Here the outer electrodes make end contacts to the nanotubes, whereas the two inner electrodes, each about 2 μm wide, are separated by 100 nm and are on the surface of the AFI crystal. As the nanotubes are only ~1 nm below the surface, which is imperfect in any case, the surface contact electrodes enable the measurement of electrical characteristics transverse to the *c*-axis of the nanotubes. In Fig. 1c and d, we show schematically the two-probe and four-probe measurement geometries. In the former the two surface-contact electrodes were used. Four-probe measurements will be presented mainly to delineate the electrical anisotropy through comparison with the two-probe results, as the difference between the two is essentially the transverse resistance. The transport measurements were carried out in the Quantum Design PPMS, with a 2.1 Ω series resistance. Both resistance and differential resistance were measured using Keithley 2182A Nanovoltmeter and 6221 AC/DC current source.

Figure 2 shows the measured resistance plotted as a function of temperature. There is a sharp drop starting at ~7.5 K, which moves to lower temperatures with applied magnetic field (perpendicular to the *c*-axis in this case). That the transition is sensitive to the magnetic field means that the superconducting behavior must originate from an array of coupled nanotubes at least a few nanometers in its transverse size [13].

Similar behavior has been observed in three different samples. In the inset to Fig. 2a, we show an enlarged upper section of the curves from 3 to 20 K. For $T > 17$ K, the curves are very good straight lines with a slight negative slope; the data shown in the inset are measured relative to this straight-line asymptote, extended to lower temperatures. They clearly show the initiation of the whole transition process starts at 15 K. While the resistance changes are small, their magnetic field dependence is unmistakable. The four-probe

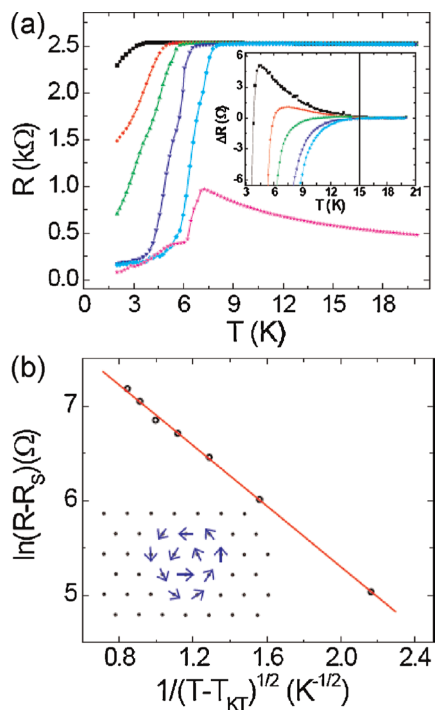

Figure 2 (online color at: www.pss-b.com) (a) Temperature dependence of two-probe resistance under a 9 T magnetic field (black), 5 T (red), 3 T (green), 1 T (dark blue), and 0 T (light blue). The magenta curve is the four-probe data at zero field. Inset: A magnified view of the upper section from 3 to 20 K with the straight-line asymptote above 17 K subtracted. The superconducting transition clearly begins at 15 K. (b) Theoretical fitting according to $\ln(R-R_S)\propto(T-T_{BKT})^{-1/2}$ for $T>T_{BKT}$, with $T_{BKT}=6.17$ K, and $R_S=1.06$ kΩ is the lower plateau resistance value in Fig. 4. It arises from the weak links connecting the different superconducting regions. Inset: A schematic picture of the transverse plane perpendicular to the *c*-axis, with each dot representing an end-view of a segment of the 1D element. A vortex excitation, indicated by arrows whose directions are given by the phase (angles) of the 1D wavefunction, is shown.

result, measured at zero field, is also displayed for comparison with the two-probe case. It is seen that the difference between the two-probe and four-probe results nearly disappeared below 5 K, indicating a clear change in the transverse resistance.

In Fig. 2b, we show the zero field resistance versus temperature data to be in excellent agreement with the prediction based on our interpretation of the 7.5 K transition as a BKT transition with a $T_{BKT} = 6.17$ K. This is a key point that will be further elaborated, together with the nonlinear IV characteristics below 7.5 K that are consistent with the manifestations of the BKT transition.

In Fig. 3, we show the magnetoresistance (MR) of the same sample at different temperatures, with the magnetic field applied perpendicular to the *c*-axis. At 2 K, there is a kink at ~2 T. The four-probe and two-probe resistances are almost identical below 2 T, but diverge above that, i.e., the transverse resistance can be turned off at $T < 6$ K and field below 2 T. Such data serve as the basis for a physical interpretation that is qualitatively different from those presented earlier [14–17] based on measurements performed on nanotube ropes, in spite of the fact that there are some similarities in the behaviors exhibited by the data. In the inset to Fig. 3, we show the observed MR anisotropy in a separate but similar sample measured at 5 T. The anisotropy means that a magnetic field perpendicular to the *c*-axis is more effective in suppressing the superconducting behavior, owing to the diamagnetic current loops that are dominantly along the *c*-axis of the nanotubes, in contrast to those that are in the transverse plane.

We consider the nanotube arrays to comprise 1D superconducting elements (either single nanotubes or small bundles of nanotubes with strong transverse coherence), each characterized with a complex Ginzburg-Landau [18] wavefunction ψ. Neighboring elements are Josephson-coupled via $-J\cos(\varphi_i - \varphi_j)$, where φ_i denotes the phase of the wavefunction for the *i*th element (inset to Fig. 2b), assumed to be constant over a finite segment of length *d*, and

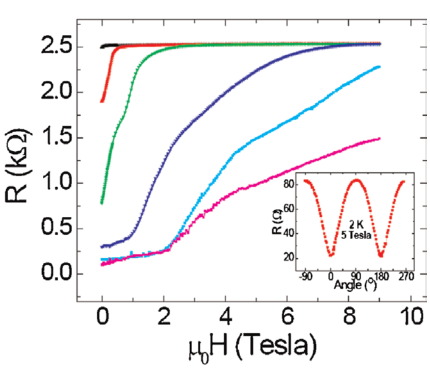

Figure 3 (online color at: www.pss-b.com) MR at 8 K (black), 7 K (red), 6 K (green), 4 K (dark blue), and 2 K (light blue). The magenta curve is the four-probe data at 2 K. Inset: MR anisotropy measured on another but similar sample; the angle is between the magnetic field and the *c*-axis.

J is proportional to superconducting electron density $|\psi|^2$. The coupled system is equivalent to a 2D spin model in the transverse plane.

As the Josephson coupling involves the transfer of charges, a natural consideration is the competing mechanism of the (Coulomb) charging effect, which is governed by two parameters, $\alpha_c = zJ/E_c$ [19] and $\alpha_r = h/4e^2R_n$ [20, 21], where the first parameter is the ratio of the Josephson coupling energy to the charging energy and the second parameter is related to the resistance parallel to the capacitance that is the source of the charging energy. Here $z = 6$ is the number of nearest neighbors, $E_c = (2e)^2/2\varepsilon C$ is the charging energy for a Cooper pair, $\varepsilon = 6$ is the dielectric constant of the zeolite frame (essentially that of aluminum phosphate), R_n denotes the normal resistance (per square) in the *ab* plane, and C is the self capacitance of a conducting nanotube surrounded by other conducting nanotubes. Whereas the charging energy tends to suppress superconductivity as it would require the charge carriers (implied by the Josephson coupling) to be energetically activated, the parallel resistance tends to favor superconductivity since the latter enhances electron delocalization. In our sample, $\alpha_r = h/4e^2R_n = 1.25$ (for $R_n = 5133\ \Omega/\square$ as estimated below). For these values of α_r superconductivity is known to always exist at low enough temperatures. But for $\alpha_r = 0$ (i.e., normal resistance $= \infty$), the criterion for the existence of superconductivity is $\alpha_c \geq 1$. Since C in this case is in the form of C_0L, where C_0 is a dimensionless constant and L is the length of the conducting nanotube, for $L \rightarrow \infty$ the charging energy is zero and therefore the condition $\alpha_c \geq 1$ is always satisfied. Hence the condition $\alpha_c = zJ/E_c > 1$ may be translated into a requirement for the minimum length of the conducting nanotube segment in the limit of infinite (transverse) normal resistance. A finite element calculation yields $C_0 = 0.27$, implying $L \geq 1.5\ \mu$m if the normal resistance is infinite. However, the existence of a finite and fairly low normal resistance in the present case, with $\alpha_r = 1.25$, means a smaller lower bound for L.

In 2D spin systems, there can be a BKT transition involving the binding–unbinding of vortex excitations [22, 23]. It has been widely observed in superconducting thin films. More recently, the appearance of BKT transition was also reported in bulk 3D high T_c superconductors [24–29].

We attribute the large resistance drop seen at 7.5 K, together with the vanishing of the transverse contact resistance below 6 K, to result from a BKT transition that establishes quasi long range order in the transverse plane [30], leading to the quench of longitudinal fluctuations and the formation of 3D coherent regions connected by weak links. Global coherence is attained at even lower temperatures. It is known that the BKT transition occurs at a temperature below the main specific heat peak [31–34] that reflects the growth of the transverse coherence. Hence this attribution is consistent with the previous specific heat results [3]. It should be noted that the present BKT transition is physically very different from the one with the same name presented earlier [35].

For our transverse-plane BKT transition, the effect of the magnetic field is mainly due to its influence on J through the suppression of superconducting electron density, which has the effect of both shifting T_{BKT} to lower temperatures as well as diminishing the magnitude of the resistance drop associated with the transition.

In Fig. 4, we show measured differential resistance plotted as a function of the current. A notable aspect of the data is the existence of two resistance plateaus at the large current limit, one at 1 kΩ and the other at 2.3 kΩ. The latter is associated with the BKT transition starting at 7.5 K. A particularly instructive curve in Fig. 4 is the one at 6 K (blue), which shows the bottom of the BKT transition's quasigap to coincide with the 1 kΩ plateau. This is consistent with the physical picture that the 1 kΩ resistance is associated with the weak links connecting the 3D superconducting regions. It also justifies treating the 1 kΩ plateau as the reference from which the BKT transition's transverse plane resistance is to be measured.

As the temperature is lowered below 7.5 K, a triangular-shaped quasigap is seen to develop. The resistance in the $I \rightarrow 0$ limit, measured relative to the 1 kΩ plateau, is predicted to vary with temperature as [36, 37] $R - R_S = 10.8bR_N\exp\{-2[b(T_{c0} - T_{BKT})/(T - T_{BKT})]^{1/2}\}$ for $T > T_{BKT}$. Here $R_S = 1.06\,\mathrm{k\Omega}$ is the lower plateau resistance and $T_{c0} = 7.5\,\mathrm{K}$ is the mean field transition temperature below which there can be nonlinear IV characteristics. In Fig. 2b, we show our data to be in excellent agreement with the above prediction. The parameter values obtained are $T_{BKT} = 6.17\,\mathrm{K}$, $b = 0.48$, and $R_N = 0.98\,\mathrm{k\Omega}$ for the normal sheet resistance.

As the measuring current I increases from 0, the triangular gap at $T < T_{c0} = 7.5\,\mathrm{K}$ means that there is a regime where R varies linearly as a function of I, implying $V \propto I^2$. The progressive variation from a constant R at 7.5 K to a triangular quasigap ($V \propto I^2$) and then to a more rounded gap at below 6.5 K, is consistent with the BKT transition behavior of $V \propto I^\alpha$ with an α varying from 1 (at the mean field transition temperature T_{c0}) to 3 (at T_{BKT}) or larger with decreasing temperature [32, 38]. From our data $\alpha = 3$ occurs at $6\,\mathrm{K} < T < 6.5\,\mathrm{K}$, which is consistent with our estimate of $T_{BKT} = 6.17\,\mathrm{K}$ (Fig. 2b). At 6 K and below, a smaller gap is seen to develop which is associated with the 1 kΩ weak link turning superconducting. At 2 K, a supercurrent gap becomes well-defined, together with the sharp peaks at the gap boundaries that signify the existence of a critical current density at which voltage first appears.

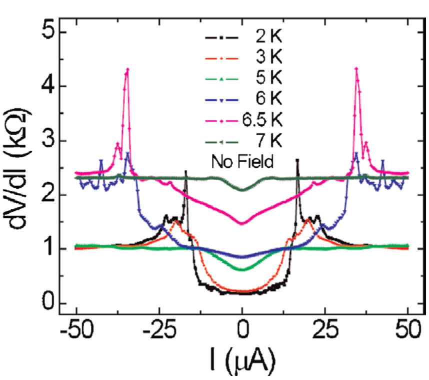

Figure 4 (online color at: www.pss-b.com) Current dependence of the differential resistance. The supercurrent gap (i.e., the low resistance region) of 2 K disappears in stages when temperature increases. Above 6 K, transverse coherence deteriorates, and the shape of the quasigap is a reflection of the BKT transition's nonlinear I–V behavior at $T < T_{c0}$.

Based on the physical interpretation presented above, we give some estimates of the relevant physical parameters.

(1) Josephson coupling energy J:

From $\pi J/k_B T_{BKT} \approx 1.12$ (Eq. (58) in Ref. [5]) and $T_{BKT} = 6.2\,\mathrm{K}$, we obtain $J = 0.19\,\mathrm{meV}$.

(2) Critical Josephson current I_c:

From $I_c = 2eJ/\hbar$, we obtain $I_c \approx 0.092\,\mu\mathrm{A}$.

(3) Normal resistance R_n per square in the transverse plane:

From $T_{BKT}/T_{c0} = [1 + 0.173R_n/(\hbar/e^2)]^{-1}$ (Eq. (9) in Ref. [23]) and $T_{BKT} = 6.2\,\mathrm{K}$, $T_{c0} = 7.5\,\mathrm{K}$ we obtain $R_n = 5133\,\Omega/\square$. This value has been used in calculating the value of $\alpha_r = 1.2$ above. The value of R_n should be compared with those of R_N obtained from fitting the temperature dependence in Fig. 2b. Differences between the two are interpreted as being due to the (non-square) aspect ratio of the superconducting regions in the *ab* plane.

(4) Superconducting gap parameter Δ at the transition temperature:

From $I_c = [\pi\Delta(T_{BKT})/2eR_n]\tanh[\Delta(T_{BKT})/2k_B T_{BKT}]$ (Ref. [39]), we obtain $\Delta(T_{BKT} = 6.2\,\mathrm{K}) \approx 0.6\,\mathrm{meV}$.

(5) Number of participating nanotubes:

In Fig. 4, there are two critical currents. The smaller one with the value of 16.8 μA (black curve, 2 K) is the Josephson critical current responsible for overcoming the weak links along the *c*-axis. The larger one with the value of 36.0 μA (blue curve, 6 K) may be regarded as the critical current for the BKT transition.

From $I_0 = 36\,\mu\mathrm{A} = wek_B T_{BKT}/\hbar\xi_c$ (Eq. (36b) in Ref. [36]), we have $I_0 = 36\,\mu\mathrm{A} = w/\xi_c \times 0.129\,\mu\mathrm{A}$ where w/ξ_c gives the effective number of participating Josephson junctions contacted by the surface electrode. Since 0.129 μA is roughly the critical current I_c estimated above (both are on the order of 0.1 μA), we take $\xi_c = 1.37\,\mathrm{nm}$ to be the unit cell length, implying $w \approx 382\,\mathrm{nm}$ along the transverse plane that is parallel to the sample–surface electrode interface. Along the depth direction (in the transverse *ab* plane but perpendicular to the surface electrode), we note that from the fit to the measured temperature variation of the resistance we have $R_N = 980\,\Omega/2 = 490\,\Omega$ (the factor of 2 comes from the consideration of the return path to the surface electrode). Since $R_n = 5133\,\Omega/\square$ as estimated above, a comparison between the two values implies an effective aspect ratio of

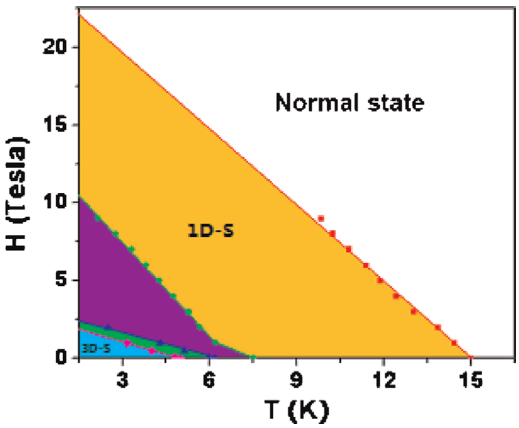

Figure 5 (online color at: www.pss-b.com) Magnetic field–temperature phase diagram summarized from the experimental data. Here yellow, violet, green, and blue regions denote, respectively, from the upper right to lower left, the fluctuating 1D superconducting regime (1D-S), the nonlinear I–V regime, the regime in which the 3D superconducting regions are connected by weak links, and the global coherence regime (3D-S) which is at the inner most lower left corner.

$\sim$10.5 between the width and depth. Therefore the effective sample size in the depth direction is $\sim$36 nm. Taken together, we estimate that there are $\sim$7460 nanotubes participating in the observed superconducting transition.

In Fig. 5, we use the perpendicular field data of the sample plot a magnetic field–temperature phase diagram. Here yellow denotes the 1D fluctuating superconductor regime, the green line denotes T_{c0} and the blue line denotes T_{BKT}, both associated with the BKT transition. Area colored by violet is the regime where one expects to see nonlinear I–V characteristics. Green is the regime in which the sample is characterized by inhomogeneous 3D superconducting regions connected by (normal) weak links. The bottom left corner is the regime of global coherence. Here symbols are data, with the connecting solid line used to delineate the different regimes.

The necessity of close electrode separations for the observation of superconducting behavior indicates that in most conducting nanotube samples electrons may be 1D localized, thus masking their intrinsic characteristics at the scale of 0.5 μm or larger.

Acknowledgements We thank B. Zhang, F. Jiang, and O. Tang for technical support. P. S. thanks Qiucen Zhang for helpful discussions. This work was supported by the Research Grants Council of Hong Kong Grants HKUST9/CRF/08, CA04/05.SC02, plus DSCI04/05.SC01 and VPAAO04/05.SC01.

References

[1] L. X. Benedict, V. H. Crespi, S. G. Louie, and M. L. Cohen, Phys. Rev. B **52**, 14935 (1995).
[2] Z. K. Tang, L. Z. Zhang, N. Wang, X. X. Zhang, G. H. Wen, G. D. Li, J. N. Wang, C. T. Chan, and P. Sheng, Science **292**, 2462 (2001).
[3] R. Lortz, Q. C. Zhang, W. Shi, J. T. Ye, C. Y. Qiu, Z. Wang, H. T. He, P. Sheng, T. Z. Qian, Z. K. Tang, N. Wang, X. X. Zhang, J. N. Wang, and C. T. Chan, Proc. Natl. Acad. Sci. **106**, 7299 (2009).
[4] V. L. Berezinskii, Sov. Phys. JETP **32**, 493 (1971); Sov. Phys. JETP **34**, 610 (1972).
[5] J. M. Kosterlitz and D. J. Thouless, J. Phys. C, Solid State Phys. **6**, 1181 (1973).
[6] W. M. Meier and D. H. Olson, Zeolites **12**, 1 (1992).
[7] N. Wang, Z. K. Tang, G. D. Li, and J. S. Chen, Nature **408**, 50 (2000).
[8] Z. K. Tang, H. D. Sun, J. Wang, J. Chen, and G. Li, Appl. Phys. Lett. **73**, 2287 (1998).
[9] I. L. Li, G. D. Li, H. J. Liu, C. T. Chan, and Z. K. Tang, Appl. Phys. Lett. **82**, 1467 (2003).
[10] Z. M. Li, H. J. Liu, J. T. Ye, C. T. Chan, and Z. K. Tang, Appl. Phys. A **78**, 1121 (2004).
[11] H. J. Liu and C. T. Chan, Phys. Rev. B **66**, 115416 (2002).
[12] The samples were prepared in the same manner as that described in [3].
[13] This sample differs from the one whose electrical resistance vs. temperature was shown [3], which reflects the behavior of a 1D (fluctuating) superconducting bundle that presumably acts as the critical link bridging the conducting path.
[14] M. Kociak, A. Yu. Kasumov, S. Gueron, B. Reulet, I. I. Khodos, Yu. B. Gorbatov, V. T. Volkov, L. Vaccarini, and H. Bouchiat, Phys. Rev. Lett. **86**, 2416 (2001).
[15] A. Kasumov, M. Kociak, M. Ferrier, R. Deblock, S. Gueron, B. Reulet, I. Khodos, O. Stephan, and H. Bouchiat, Phys. Rev. B **68**, 214521 (2003).
[16] A. D. Martino and R. Egger, Phys. Rev. B **70**, 014508 (2004).
[17] M. Ferrier, A. D. Martino, A. Kasumov, S. Gueron, M. Kociak, R. Egger, and H. Bouchiat, Solid State Commun. **131**, 615 (2004).
[18] M. Tinkham, Introduction to Superconductivity, second ed. (MGH, New York, 1996), chap. 4.
[19] F. P. Mancini, P. Sodano, and A. Trombettoni, Phys. Rev. B **67**, 014518 (2003).
[20] S. Chakravarty, S. Kivelson, and G. T. Zimanyi, Phys. Rev. B **35**, 7256 (1987).
[21] A. Kampf and G. Schon, Phys. Rev. B **36**, 3651 (1987).
[22] S. Doniach and B. A. Huberman, Phys. Rev. Lett. **42**, 1169 (1979).
[23] M. R. Beasley, J. E. Mooij, and T. P. Orlando, Phys. Rev. Lett. **42**, 1165 (1979).
[24] S. Martin, A. T. Fiory, R. M. Fleming, G. P. Espinosa, and A. S. Cooper, Phys. Rev. Lett. **62**, 677 (1989).
[25] L. N. Bulaevskii, M. Ledvij, and V. G. Kogan, Phys. Rev. Lett. **68**, 3773 (1992).
[26] Y. Matsuda, S. Komiyama, T. Onogi, T. Terashima, K. Shimura, and Y. Bando, Phys. Rev. B **48**, 10498 (1993).
[27] B. Chattopadhyay and S. R. Shenoy, Phys. Rev. Lett. **72**, 400 (1994).
[28] R. Sugano, T. Onogi, and Y. Murayama, Phys. Rev. B **48**, 13784 (1993).
[29] A. K. Pradhan, S. J. Hazell, J. W. Hodby, C. Chen, Y. Hu, and B. M. Wanklyn, Phys. Rev. B **47**, 11374 (1993).

[30] As the occupation fraction for the superconducting nanotubes in the transverse plane must be less than 100%, it remains an open possibility that the transition temperature could be dependent on the fraction [38,39] of superconducting nanotubes in the zeolite pores.
[31] R. Gupta and C. F. Baillie, Phys. Rev. B **45**, 2883 (1992).
[32] H. Q. Ding and M. S. Makivic, Phys. Rev. B **42**, 6827 (1990).
[33] R. Gupta, J. DeLapp, and G. G. Batrouni, Phys. Rev. Lett. **61**, 1996 (1988).
[34] J. Tobochnik and G. V. Chester, Phys. Rev. B **20**, 3761 (1979).
[35] In references [14–17], the mentioned BKT transition refers to the binding–unbinding transition of quantum phase slips of opposite helicities so that a zero-resistance state becomes possible even in a 1D superconducting wire. This is in contrast to the BKT transition in the transverse plane that mediates a 1D to 3D crossover.
[36] B. I. Halperin and D. R. Nelson, J. Low Temp. Phys. **36**, 599 (1979).
[37] D. W. Abraham, C. J. Lobb, M. Tinkham, and T. M. Klapwijk, Phys. Rev. B **26**, 5268 (1982).
[38] A. F. Hebard and A. T. Fiory, Phys. Rev. Lett. **20**, 1603 (1983).
[39] V. Ambegaokar and A. Baratoff, Phys. Rev. Lett. **10**, 486 (1963); Phys. Rev. Lett. **11**, 104 (E) (1963).

